Modeling the size distribution in a fluidized bed of nanopowder

Andrea Fabre[a], Samir Salameh[a], Michiel T. Kreutzer[a], J. Ruud van Ommen[a,*]

[a]Delft University of Technology, Department of Chemical Engineering, Van der Maasweg 9, 2629 HZ Delft, the Netherlands

Abstract

Fluidization is a technique used to process large quantities of nanopowder with no solvent waste and a large gas-solid contact area. Nonetheless, nanoparticles in the gas phase form clusters, called agglomerates, due to the relatively large adhesion forces. The dynamics within the fluidized bed influence the mechanism of formation, and thus, the morphology of the agglomerates. There are many theoretical models to predict the average size of fluidized agglomerates; however, these estimates of the average lack information on the whole size range. Here, we predict the agglomerate size distribution within the fluidized bed by estimating the mode and width using a force balance model. The model was tested for titania (TiO_2), alumina (Al_2O_3), and silica (SiO_2) nanopowders, which were studied experimentally. An *in-situ* method was used to record the fluidized agglomerates for size analysis and model validation.

Keywords: Model, Size distribution, Fluidization, Agglomerate, Nanoparticle

1. Introduction

A balance between adhesion and separation forces (or energies) is a settled theoretic framework to predict the average agglomerate size of fluidized nanopowders [1–8]. The average agglomerate size is usually assumed to be that at which the adhesion and separation forces balance each other; however, predictions of agglomerate size distributions are absent. It is well known that cohesive powders form agglomerates with a very wide, typically log-normal, size distribution [9–12]. The purpose of the present paper is to explore a conceptual model to predict the width of the distribution using a force balance approach.

Fluidization is a common method to process nanoparticles [11, 13–15], which fluidize as agglomerates due to the relatively strong attractive interactions, particularly van der Waals and capillary forces [13, 16–19]. As the stable

---

*Corresponding author, Tel.: +31 15 27 84393
Email address: J.R.vanOmmen@tudelft.nl (J. Ruud van Ommen)

structures of the fluidized powder, the properties of the agglomerates are directly linked to the fluidization dynamics [13]. Nanopowder fluidization depends on the agglomerate properties and can be classified as agglomerate particulate fluidization (APF) or agglomerate bubbling fluidization (ABF) [20]. APF is characterized by uniform, non-bubbly behavior, good solid-gas contact, and homogeneous distribution of powder throughout the bed. On the other hand, ABF shows a small bed expansion with channels, bubbles, and non-uniform powder distribution [9, 15]. The fluidization type and agglomerate properties are co-dependent. As a key property distinguishing the two forms of fluidization, various studies have focused on the theoretical and experimental estimation of the fluidized agglomerate size.

Visualization techniques for the fluidized nano and micron size scales include the *ex situ* Transmision and Scanning Electron Microscopes (TEM and SEM, respectively), and multiple camera systems for *in situ* measurements. Sample extraction and preparation of the fragile fluidized agglomerates for SEM and TEM have led to images of agglomerate sizes smaller than those expected inside the fluidized bed [21]. This indicates the need of *in situ* techniques for more accurate results [21, 22]. A common *in situ* method used to measure the fluidized agglomerate size involves laser illumination and a digital CCD camera [15]. Average agglomerate sizes between 70 μm and 900 μm have been measured with this technique for Aerosil R974, Aeroxide TiO_2, fumed silica, zirconia, and iron oxide nanopowders [10, 11, 13, 21–24]. Furthermore, the laser / CCD camera system was also used for size distribution measurements at the splash zone of the Aerosil R974 fluidized bed with mode at approximately 140 μm [10] or 200 μm [11], or a positive skewed distribution in the size range 40-600 μm [22]. Another visualization technique, the Lasentec Focused Beam Reflectance Method / Particle Vision Measurement system, showed a log-normal size distributions of Aerosil R974 and Aerosil 90 [9, 25]. More recently, de Martin et al. [4] developed a settling tube technique for the analysis of agglomerate size distribution, among other properties, at the splash zone of the fluidized bed.

Knowledge of the fluidized agglomerate size distribution is crucial for proper understanding of the dynamic processes within the fluidized bed, which are of great importance in nanopowder processing and applications such as in medicine, optics, and solar cells [26, 27]. Even though the tools to experimentally determine the agglomerate size distribution are available, most of the studies only focus on the average size values. These measured sizes are mainly used for qualitative analysis or comparison based on different fluidization conditions or powder properties, with no

further description of the size distribution. This includes the limited use of force (energy) balances to estimate the mean agglomerate size only.

In this work we predict the mode and width of the log-normal fluidized agglomerate size distribution from a simple force balance. The attractive and repulsive forces were calculated theoretically to identify the dominating interactions. This model is simple, and provides a good prediction of the size distribution based on a novel interpretation of the conventional force balance concept. Simplification of the final expression obtained from the balance shows that the size distribution of fluidized nanoparticle agglomerates is self-similar. The calculated size distribution is validated by *in situ* experiments using oxide nanopowders showing either APF or ABF behavior.

2. Material and Methods

The nanopowders used in this study were bought from Evonik. The characteristics given by the supplier are shown in Table 1. The powder selection involves both fluidization behaviors, APF and ABF. As mentioned in literature, Al_2O_3 and TiO_2 show bubbling, while SiO_2 fluidized homogeneously [9, 11, 28]. All nanopowders are sieved using a 450 μm mesh to remove large agglomerates that would prevent proper fluidization. The powders are fluidized in a 15 cm high quartz column with a square cross-section of 4.5×4.5 cm using pure nitrogen gas at 0.13 m/s, which enters the column through a distributor plate. The gas leaving the setup is sent to a water bubbler and HEPA filter to remove any entrained particles.

The fluidized agglomerates are recorded while falling through a settling tube placed in the splash zone. As was demonstrated by Wang et al. [22], agglomerates present in the splash zone are representative of those found in the bed. Additionally, the gas velocity used for fluidization is large enough for the agglomerates to follow the gas flow by keeping their Stokes number bellow one. The settling tube is a black box with an opening at the top to catch falling agglomerates, and two openings on the side for agglomerate recording and tube cleaning purposes (Fig.1). A rigid borescope (Olympus R040-021-000-60 S5) and high speed camera (Phantom v9.1) system are used for the recordings, enabling a visible size range from 30 μm to 4 mm [29].

The videos are taken 10 minutes after starting fluidization to reach an observable steady state. The movies are analyzed using a MATLAB script by dividing them into frames, and later processing each frame for light correction,

and agglomerate recognition, tracking, filtering, and measurements. More details on the technique can be found in the papers by de Martin et al. [29, 30].

An important feature of nanoparticle agglomerates is the solid fraction, which can be estimated from their density. The agglomerate density can be calculated from the settling velocity and size obtained from the videos. The size distribution is taken directly from the images, assuming the agglomerates to be spherical [30]. The diameter used to describe the size of the agglomerate is the area equivalent diameter; the diameter of a circle with the same area as the region recognized from image processing. Other works suggest the use of volume-surface diameter for fluidized agglomerate sizing from 2D images as a better representation of the fluid-particle interaction [22]. However, the error propagation from image analysis is increases in this case.

The settling velocity is also directly calculated from the images since the frame rate is known, and agglomerate displacement between frames is obtained from the agglomerate recognition step. Settling velocity and agglomerate size are used to calculate the Reynolds number, which is used to estimate the drag coefficient, thus completing the list of parameters needed to determine the agglomerate density.

3. Theory

The forces acting on a fluidized agglomerate are divided into two categories: adhesion (those keeping ensembles of particles together) and separation (those breaking particle ensembles). The forces to be considered, and their classification into the two groups varies in literature. Van der Waals, capillary, and electrostatic are regularly in the adhesion group, while gravity-buoyancy sometimes is classified as cohesive [2, 3] and sometimes as a separation force [7]. Here, gravity-buoyancy is classified as a separation force. Bed expansion, drag, and collision forces belong to the group of separation forces. The gravity-buoyancy force is evaluated with the effective density of the agglomerate. The bed expansion force is that exerted on nanoparticles by the bubbles inside the bed, which depends on bubble size, agglomerate pressure around a spherical bubble, gravity, agglomerate size and density, and coordination number [1]. The drag force calculation includes a shape factor of 0.9 in the denominator, representing the agglomerate sphericity. Finally, capillary force is estimated as the maximum force assuming the formation of a liquid bridge between two highly porous spherical agglomerates. Figure 2 presents a comparison of the forces for TiO_2 P25 with properties as

shown in Table 1, contact distance of 0.4 nm, Hamaker coefficient of 1.02×10^{-19} J, Young's modulus of 234 GPa, and work of adhesion of 0.8 J/m^2, with fluidizing gas velocity of 13 cm/s. It is shown that the dominant forces acting on the fluidized agglomerate are van der Waals (F_{vdW}), capillary (F_c), and collision (F_{coll}). The difference in the values of powder properties and fluidization conditions for the studied materials don't change the order of magnitude of the forces; hence, Figure 2 is a general representation of all the nanopowders mentioned in this paper.

In a dry system, the main forces acting on a fluidized agglomerate are van der Waals and collision (Fig.3). Hence, a simple but representative force balance equating the effective forces (Eq.1) can give valuable approximations to the size distribution within the fluidized bed.

$$F_{vdW} = F_{coll} \tag{1}$$

Comparing the forces leads to two important values, the size at which the difference between the adhesion and separation forces is maximum, and that at which it is zero (Fig.4). A crucial concept of this model is that agglomeration is fastest when the difference between adhesion and separation forces is largest. The agglomerate size where this occurs has the steepest slope in the log-normal size distribution (i.e. inflection point). A force difference of zero indicates that the average separation and adhesion forces have the same magnitude, so that a force unbalance leads to a probability density fall onto smaller or larger sizes. Hence, the size at zero difference is the mode, denoting a threshold on the distribution.

3.1. Van der Waals force

When two soft bodies are pulled together by attractive forces, there is a flattening at the location of contact [31]. Therefore, the force between two soft bodies includes the interaction between the deformed adhesive areas, and that between the volumes within the van der Waal's range. Using the assumptions of small non-elastic deformation, absence of electrostatic components, and smooth surfaces, the contact force can be expressed as [32]:

$$F_{vdW} = \frac{h_w \phi R_a}{16\pi\delta^2}\left(1 + \frac{h_w\phi}{8\pi^2\delta^3 H_r}\right) \tag{2}$$

5

where h_w is the Lifshitz-van der Waals constant ($h_w = \pi H_a 3/4$), R_a is the agglomerate radius, ϕ is the solid fraction of the agglomerate, δ is the contact distance commonly taken as $0.4nm$ [32], and H_r is the agglomerate Young's modulus calculated using [33]:

$$H_r = 17.1\phi^4 \left[\frac{E_p^2 \Gamma}{d_p}\right]^{1/3} \tag{3}$$

which depends on the nanoparticle's Young's modulus (E_p), work of adhesion (Γ), and diameter (d_p) [34]. The Hamaker coefficient (H_a) [35] used to calculate h_w is an average of those considering water or vacuum as the medium, given that water molecules cannot be completely removed from the nanoparticle surface [36]. Since the Hamaker coefficient is estimated by integrating the van der Waals' attractive potential over the volume and number of molecules, for porous structures, the attraction depends on the solid fraction. Therefore, the Lifshitz-van der Waals constant is multiplied by the solid fraction (ϕ) to account for the void of the agglomerate when calculating the contribution of the interaction. This results in the final expression of the van der Waals force between two soft porous agglomerates (Eq.2).

3.2. Collision force

Due to the dynamics within a fluidized bed, agglomerates are constantly colliding with each other. The collision force is derived from the theory of elasticity [37] for agglomerates colliding vertically. The collision force depends on the degree of compression, which is a function of the density (ρ_a), Young's modulus (H_r), Poisson's ratio (ν), size (d_a), and relative collision velocity (V_x) of the agglomerates. The following expression assumes the agglomerates to be identical spheres colliding in a fluid with viscosity μ and density ρ_f, represented as [2, 3, 5, 7]:

$$F_{coll} = 0.166 \left(\frac{\pi V_x^6 \rho_a^3}{k^2}\right)^{1/5} d_a^2 \tag{4}$$

where

$$k = \frac{1 - \nu^2}{\pi H_r} \tag{5}$$

6

The estimated relative velocity of the agglomearte depends on the fluidization behavior. That for ABF powders is [7, 38]:

$$V_b = (1.5\bar{P}_{s,n}D_b g\epsilon_b)^{0.5} \tag{6}$$

where $\bar{P}_{s,n}$ is the dimensionless average particle pressure of a non-sticky system taken as 0.077 [18, 39], g is the acceleration due to gravity, ϵ_b is the void fraction of the fluidized bed, and D_b is the bubble diameter estimated by [38]:

$$D_b = 0.652(A_t(u_0 - u_{mf}))^{2/5} \tag{7}$$

from the bed cross-sectional area (A_t), superficial gas velocity (u_0), and minimum fluidization velocity (u_{mf}), which can be calculated from [38, 40]:

$$u_{mf} = \frac{0.00923d_a^{1.82}(\rho_a - \rho_f)^{0.94}}{\mu^{0.88}\rho_f^{0.06}} \tag{8}$$

In the case of non-bubbling fluidization (APF), the relative velocity is expected to range between ≈ 0 and the agglomerate settling velocity (Stokes regime) plus the superficial gas velocity. The lower limit is for two suspended agglomerates that barely come into contact in a close-to-parallel trajectory. The upper limit is for an agglomerate moving downwards at its settling velocity colliding with an upward moving agglomerate at the velocity of the fluidizing gas. Considering the relative velocity for non-bubbling fluidization to have a symmetric distribution, it comes down to:

$$V_{nb} \approx \frac{1}{2}\left[u_0 + \frac{(\rho_a - \rho_f)d_a^2 g}{18\mu}\right] \tag{9}$$

3.3. Size Distribution Prediction

To simplify the complexity of fluidized nanoparticle agglomerates, the model includes some basic assumptions. Only collision and van der Waals, the two dominating forces acting on a dry fluidized agglomerate, are considered.

Agglomerates are assumed to be spherical with an homogeneous distribution of nanoparticles. The two interacting agglomerates described throughout the model are assumed to be identical. For the model, all collisions are assumed to be head-to-head at an angle of $180°$. The assumptions that have the greatest impact on the accuracy of the model prediction are those affecting the elasticity of the agglomerates, which has a strong dependence on the agglomerate's density, or agglomerate solid fraction, as seen in Eq.3. From the given assumptions, the final overall force difference for our model becomes:

$$\Delta F = \frac{h_w \phi}{32\pi\delta^2}\left(1 + \frac{h_w \phi}{8\pi^2\delta^3 H_r}\right)d_a - 0.166\left(\frac{\pi V_x^6 \rho_a^3}{k^2}\right)^{1/5} d_a^2 \tag{10}$$

From Equations 2-9 it is clear that h_w, δ, k, H_r, and ρ_a are constant, and V_x hardly changes with size. Therefore, the force balance has the form:

$$\Delta F = ad_a - bd_a^n \tag{11}$$

where b and n depend on the fluidization behavior. Given that the 1 inside the first parenthesis of Eq.10 (van der Waals) was found to have minimal contribution, the second term became the coefficient a:

$$\frac{h_w^2 \phi^2}{256\pi^3\delta^5 H_r} = a \tag{12}$$

In the case of bubbling fluidization (ABF), minimum fluidization velocity (u_{mf}) depends on agglomerate size (d_a) to the power of 1.82 (Eq.8). Once u_{mf} is evaluated and compared to the superficial gas velocity (u_0), it is found to be 2 orders of magnitude smaller, and thus, neglected. The coefficient b is then evaluated from:

$$D_b \approx 0.652(A_t(u_0))^{2/5} \tag{13}$$

$$V_b \approx (1.5\bar{P}_{s,n}D_b g\epsilon_b)^{0.5} \tag{14}$$

$$0.166\left(\frac{\pi V_b^6 \rho_a^3}{k^2}\right)^{1/5} = b \tag{15}$$

8

giving a simplified model to predict the size distribution by estimating the agglomerate size at maximum and zero force difference (ΔF) corresponding to the size at the inflection point ($d_{a(MaxG)}$) and mode ($d_{a(Mode)}$), respectively:

$$\Delta F = 0 = ad_a - bd_a^2 \quad \longrightarrow \quad d_{a(Mode)} = (a/b) \tag{16}$$

$$\frac{d\Delta F}{dd_a} = 0 = a - 2bd_a \quad \longrightarrow \quad d_{a(MaxG)} = (a/2b) \tag{17}$$

In the case of non-bubbling fluidization (APF), the velocity expression was fully substituted in the force balance equation, leading to:

$$0.166 \left(\frac{\pi(\frac{1}{2}\left[u_0 + \frac{(\rho_a - \rho_f)g}{18\mu}\right])^6 \rho_a^3}{k^2} \right)^{1/5} = b \tag{18}$$

which results in the following set of expressions:

$$\Delta F = 0 = ad_a - bd_a^{22/5} \quad \longrightarrow \quad d_{a(Mode)} = (a/b)^{5/17} \tag{19}$$

$$\frac{d\Delta F}{dd_a} = 0 = a - (22/5)bd_a^{17/5} \quad \longrightarrow \quad d_{a(MaxG)} = (a/b)^{5/17}(5/22)^{5/17} \tag{20}$$

The mode size depends on constant parameters from material properties and fluidization conditions represented by a and b. The size at the inflection point is half the mode in ABF powders, and close to 0.65 for APF systems. This characteristic holds if the average relative particle velocity in ABF is independent of agglomerate size. The self-similarity in the size distribution of fluidized agglomerates is expected since experimental data of micron size particulate systems shows the same trend [41, 42]. Furthermore, the mathematical feature of the collision kernels in the Smoluchowski differential equation for fractal-like agglomerates are such that self-similar size distributions are possible [43–45].

The a/b ratio includes the Hamaker coefficient, Young's modulus, relative particle velocity, and solid fraction. This ratio indicates that increasing the Hamaker coefficient will increase the mode size, which is expected as the adhesion force is increased. Additionally, increasing the Young's modulus, relative particle velocity, or solid fraction will decrease the mode and distribution width. This is also foreseen since harder agglomerates present less deformation during collision, creating a small area of contact, thus dissipating little energy on deformation and using most of it on breakage. Moreover, the model indicates that fluidization gas velocity has minor effect on the agglomerate size, which is experimentally observed in Quevedo et al. [25], for conventional fluidization of nanopowders.

4. Results and Discussion

4.1. Size Distribution

The size distribution of the fluidized agglomerates was experimentally determined from the images taken by the settling tube technique [29]. For all the powders, the agglomerate size varies between 76 μm and 462 μm, which is in good agreement with values found in literature using a high speed camera [10, 11, 13, 21, 22]. The density distribution can be calculated once the size and agglomerate settling velocity are known. The number-based average size and density values for all powders are presented in Table 2.

Experimental studies of nanoparticle agglomerates from literature have reported a log-normal size distribution [9, 25, 46]. This is expected, because for granulation, which is similar to nanoparticle agglomeration [41, 44, 47, 48], the coalescence principle also predicts a log-normal size distribution. Indeed, we found experimentally that a log-normal distribution best described the size distribution for all nanopowders.

4.2. Model Predictions

Now, the agreement between the size distribution based on the model presented above and the experimental data is analyzed. The values used to calculate the a and b coefficients for each powder are presented in Table 3. There are two interesting aspects to consider. First, the model predicts that bubbling fluidization leads to a size distribution with a mode to infection point ratio δ of 0.5, whereas homogeneous fluidization gives a ratio of $\delta = 0.65$. The second prediction is the absolute values of agglomerate sizes. It should be noted that the model predicts these features of

the agglomerate size distribution without any fitted parameters, and that it uses independently determined material properties for the different powders.

Table 4 shows key parameters describing the log-normal distribution for our own data and for powders from other studies. Considering first the bubbling fluidization, the average value of δ is found to be 0.51, close to the theoretical prediction of 0.5. Similarly, the data obtained for homogeneous fluidization has $\langle \delta \rangle = 0.58$, comparable to the model value of 0.65. The agreement is not perfect, and there is still significant variation among the systems within each group. Nonetheless, the data strongly suggests that the type of fluidization is an important factor in determining this important characteristics of the distribution.

Since it has been established that the dimensionless features of the distribution agree with the model, the absolute size predictions are now evaluated. Note that this is essentially based on a single number for each powder, i.e. the ratio of a and b in Eq 11. Fig.5 shows the experimental histograms, together with the model predictions. The experimental values of μ, σ and δ are presented in Table 3, while the model values are $(\mu, \sigma, \delta) = (4.88, 0.387, 0.50)$ for TiO$_2$, $(5.61, 0.387, 0.51)$ for Al$_2$O$_3$, and $(5.47, 0.312, 0.60)$ for SiO$_2$. Taking into consideration that there are no fitted parameters, the agreement is notably good. An important caveat, however, is the use of the experimentally determined density, of which the uncertainty propagates strongly into the uncertainty of the predicted size. The distributions obtained from the model by keeping density as a fitting parameter are included in Appendix B. Still, Fig.5 is the more impressive demonstration of the importance of the model.

5. Conclusions

A simple model based on a separation versus adhesion force balance was developed to estimate the size distribution in a fluidized bed of nanopowder. The model predicts two key values from which the fluidized agglomerate log-normal size distribution can be evaluated. One value is the size at the inflection point, determined as that at which the difference between the adhesion and separation forces is maximum. And the second being the mode size, that at which separation and adhesion forces balance each other. The two sizes are related by a factor of 0.5 and 0.65, for ABF and APF, respectively. The model was validated with experiments using three commercial metal oxide nanopowders and data from literature showing both, bubbling (ABF) and uniform (APF), fluidization behaviors. The prediction of the

size distribution is quite close to the experimental data. Nonetheless, further refinement is required for applicability to hydrophobic materials and inclusion of clusters smaller than 10 μm.

Acknowledgments

Nomenclature

a	Force balance coefficient
A_t	Bed cross-sectional area $[m^2]$
b	Force balance coefficient
c	Force balance exponent
d_a	Agglomerate size $[m]$
$d_{a(MaxG)}$	Fluidized agglomerate diameter at the distribution's inflection point $[m]$
$d_{a(Mode)}$	Fluidized agglomerate mode diameter $[m]$
D_b	Bubble size $[m]$
D_f	Agglomerate fractal dimension
d_p	Nanoparticle diameter $[m]$
E_p	Nanoparticle Young's modulus [Pa]
g	Gravitational acceleration $[m_s^2]$
H_a	Hamaker coefficient $[J]$
H_r	Agglomerate Young's modulus $[Pa]$
h_w	Lifshitz-van der Waals constant $[J]$
K	Function of Poisson's ratio and Young's modulus
k_n	Agglomerate prefactor
N_p	Number of particles in an agglomerate

$\bar{P}_{s,n}$	Dimensionless particle pressure
R_a	Agglomerate radius $[m]$
R_{tip}	Colloid radius $[m]$
s	Indentation depth $[m]$
s_0	Point of zero indentation $[m]$
$u_m f$	Minimum fluidization velocity $[m/s]$
u_o	Superficial gas velocity $[m/s]$
V_x	Collision relative velocity $[m/s]$
F_{Hertz}	Hertz force $[N]$
F_{vdW}	Van der Waals force $[N]$
F_{coll}	Collision force $[N]$
ϵ_a	Agglomerate void fraction
ϵ_b	Fluidized bed void fraction
δ	Separation at contact $[m]$
ΔF	Adhesion and separation force difference $[N]$
γ	Water surface tension $[N/m]$
Γ	Work of adhesion $[J/m^2]$
μ	Fluid viscosity $[N]$
ν	Agglomerate Poisson's ratio
ρ_a	Agglomerate density $[kg/m_3]$
ρ_f	Fluid density $[kg/m^3]$
ρ_p	Nanoparticle density $[kg/m^3]$
ρ_{Tamped}	Nanopowder bulk density $[kg/m^3]$
ϕ	Agglomerate shape factor

Appendix A. LogNormal Distribution from Predicted Values

A log-normal distribution profile was found to be the best standardized fit for all the nanopowders. The relevant equations are shown in this section. The so called "Inflection Point" value corresponds to the size at which adhesion and separation forces have the largest difference. Thus, this is expected to be the size where growth rate is maximum ($\frac{d^2 LogNormalPDF}{dx^2}$). The "Mode" agglomerate size calculated by the model is that at which separation and adhesion forces balance each other. The set of equations is:

$$LogNormalPDF = \frac{1}{x\sigma\sqrt{2\pi}}e^{-\frac{(lnx-\mu)^2}{2\sigma^2}} \qquad\qquad Mode = e^{\mu-\sigma^2} \qquad\qquad (A.1)$$

$$MaxGrowthRate = e^{\frac{1}{4}(\pm\sqrt{4\sigma^4+16\sigma^2}-6\sigma^2+4\mu)} \qquad\qquad Variance = (e^{\sigma^2}-1)e^{2\mu-\sigma^2} \qquad (A.2)$$

$$Mean = e^{\mu+\frac{\sigma^2}{2}} \qquad\qquad Median = e^{\mu} \qquad\qquad (A.3)$$

Vitae

- Andrea Fabre has a Bachelor in Biological and Chemical Engineering from the Massachusetts Institute of Technology. She is currently pursuing her PhD. at Delft University of Technology in the Department of Chemical Engineering working on nanoparticle interactions and dynamic behavior during fluidization.

- Samir Salameh is a postdoc at the Delft University of Technology in the department of Chemical Engineering. He received his PhD on Contact behavior of metal oxide aggregates from the University of Bremen in 2015. His current research interests are nanoparticle contact forces and fluidization.

- Michiel T. Kreutzer is a professor and Department Head of Chemical Engineering at the Delft University of Technology, from where he also received his PhD. He has been recognized as an outstanding teacher and scientist. His research interests include multiphase microfluidics, transport phenomena in miniaturized systems, microreactor engineering, and heterogeneous catalysis.

- J. Ruud van Ommen is a professor at the Delft University of Technology in the department of Chemical Engineering, from where he has a PhD. He has received multiple grants and awards while working on dispersed multiphase flows, nanostructured materials, scalable processes, nanotechnology, and atomic layer deposition.

[1] M. H. Yuki Iwadate, Prediction of agglomerate sizes in bubbling fluidized beds of group c powders, Powder Technology 100 (1998) 223–236.

[2] T. Zhou, H. Z. Li, Force balance modelling for agglomerating fluidization of cohesive particles, Powder Technology 111 (2000) 60–65.

[3] D. Turki, N. Fatah, Behavior and fluidization of the cohesive powders: Agglomerates sizes approach, Brazilian Journal of Chemical Engineering 25 (4) (2008) 697–711.

[4] L. de Martin, W. G. Bouwman, J. R. van Ommen, Multidimensional nature of fluidized nanoparticle agglomerates, Langmuir 30 (42) (2014) 12696–12702.

[5] H. L. Tao Zhou, Estimation of agglomerate size for cohesive particles during fluidization, Powder Technology 101 (1999) 57–62.

[6] M. R. Tamadondar, R. Zarghami, K. Boutou, M. Tahmasebpoor, N. Mostoufi, Size of nanoparticle agglomerates in fluidization, The Canadian Journal of Chemical Engineering 94 (3) (2016) 476–484.

[7] S. Matsuda, H. Hatano, T. Muramoto, A. Tsutsumi, Modeling for size reduction of agglomerates in nanoparticle fluidization, AIChE Journal 50 (11) (2004) 2763–2771.

[8] J. Chaouki, C. Chavarie, D. Klvana, Effect of interparticle forces on the hydrodynamic behavior of fluidized aerogels, Powder Technology 43 (2) (1985) 117–125.

[9] J. A. Quevedo, A. Omosebi, R. Pfeffer, Fluidization enhancement of agglomerates of metal oxide nanopowders by microjets, AIChE Journal 56 (6) (2010) 1456–1468.

[10] M. A. S. Valverde, J. M.and Quintanilla, A. Castellanos, D. Lepek, J. Quevedo, R. N. Dave, R. Pfeffer, Fluidization of fine and ultrafine particles using nitrogen and neon as fluidizing gases, AIChE Journal 54 (2008) 86–103.

[11] C. Zhu, Q. Yu, R. N. Dave, R. Pfeffer, Gas fluidization characteristics of nanoparticle agglomerates, AIChE Journal 51 (2005) 426–439.

[12] S. V. Sokolov, E. Kätelhön, R. G. Compton, A thermodynamic view of agglomeration, The Journal of Physical Chemistry C 119 (44) (2015) 25093–25099.

[13] L. F. Hakim, J. L. Portman, M. D. Casper, A. W. Weimer, Aggregation behavior of nanoparticles in fluidized beds, Powder Technology 160 (3) (2005) 149–160.

[14] A. Goulas, J. Ruud van Ommen, Atomic layer deposition of platinum clusters on titania nanoparticles at atmospheric pressure, J. Mater. Chem. A 1 (2013) 4647–4650.

[15] J. R. van Ommen, J. M. Valverde, R. Pfeffer, Fluidization of nanopowders: a review, J Nanopart Res 14 (2012) 737.

[16] J. Israelachvili, Intermolecular and surface forces, Academic Press, 1991.

[17] J. R. van Ommen, Manufacturing core-shell nanoparticles by atomic layer deposition in a fluidized bed, in: International Symposium on Chemical Reaction Engineering, 2012.

[18] J. Shabanian, R. Jafari, J. Chaouki, Fluidization of ultrafine powders, Inter. Review of Chemical Eng. 4 (2012) 16–50.

[19] M. J. Espin, J. M. Valverde, M. A. S. Quintanilla, A. Castellanos, Electromechanics of fluidized beds of nanoparticles, Physical Review E 79 (1) (2009) 011304.

[20] W. Yao, G. Guangsheng, W. Fei, W. Jun, Fluidization and agglomerate structures of sio2 nanoparticles, Powder Technology 124 (2002) 152–159.

[21] C. H. Nam, R. Pfeffer, R. N. Dave, S. Sundaresan, Aerated vibrofluidization of silica nanoparticles, AIChE Journal 50 (2004) 1776–1785.

[22] X. S. Wang, V. Palero, J. Soria, M. J. Rhodes, Laser-based planar imaging of nano-particle fluidization: Part i-determination of aggregate size and shape, Chemical Engineering Science 61 (2006) 5476–5486.

[23] H. Liu, L. Zhang, T. Chen, S. Wang, Z. Han, S. Wu, Experimental study on the fluidization behaviors of the superfine particles, Chemical Engineering Journal 262 (2015) 579 – 587.

[24] X. S. Wang, F. Rahman, M. J. Rhodes, Nanoparticle fluidization and geldart's classification, Chemical Engineering Science 62 (2007) 3455–3461.

[25] J. A. Quevedo, R. Pfeffer, In situ measurements of gas fluidized nanoagglomerates, Industrial and Engineering Chemistry Research 49 (2010) 5263–5269.

[26] J. M. Zook, V. Rastogi, R. I. MacCuspie, A. M. Keene, J. Fagan, Measuring agglomerate size distribution and dependence of localized surface plasmon resonance absorbance on gold nanoparticle agglomerate size using analytical ultracentrifugation, ACS Nano 5 (10) (2011) 8070–8079.

[27] N. Mandzy, E. Grulke, T. Druffel, Breakage of tio2 agglomerates in electrostatically stabilized aqueous dispersions, Powder Technology 160 (2) (2005) 121 – 126.

[28] J. Scicolone, D. Lepek, L. Louie, R. Dav, Fluidization and mixing of nanoparticle agglomerates assisted via magnetic impaction, Journal of Nanoparticle Research 15 (2) (2013) 1–21. doi:10.1007/s11051-013-1434-7.
URL http://dx.doi.org/10.1007/s11051-013-1434-7

[29] L. de Martin, J. Sanchez-Prieto, F. Hernandez-Jimenez, J. van Ommen, A settling tube to determine the terminal velocity and size distribution of fluidized nanoparticle agglomerates, Journal of Nanoparticle Research 16 (1) (2013) 2183.

[30] L. de Martin, A. Fabre, J. R. van Ommen, The fractal scaling of fluidized nanoparticle agglomerates, Chemical Engineering Science 112 (0) (2014) 79 – 86.

[31] B. Dahneke, The influence of flattening on the adhesion of particles, Journal of Colloid and Interface Science 40 (1) (1972) 1 – 13.

[32] H. Krupp, Particle adhesion theory and experiment, Advances in Colloid and Interface Science 1 (2) (1967) 111 – 239.

[33] K. Kendall, N. M. Alford, J. D. Birchall, Elasticity of particle assemblies as a measure of the surface energy of solids, Proceedings of the Royal Society of London A: Mathematical, Physical and Engineering Sciences 412 (1843) (1987) 269–283.

[34] A. Fabre, S. Salameh, L. C. Ciacchi, M. T. Kreutzer, J. R. van Ommen, Contact mechanics of highly porous oxide nanoparticle agglomerates, Journal of Nanoparticle Research 18 (7) (2016) 1–13.

[35] H. J. Butt, M. Kappl, Surface and Interfacial Forces, Wiley, 2010.

[36] S. Salameh, J. Schneider, J. e. a. Laube, Adhesion mechanisms of the contact interface of tio2 nanoparticles in films and aggregates, Langmuir 28 (2012) 11457–11464.

[37] J. G. S.P. Timoshenko, Theory of Elasticity, McGraw-Hill, 1970.

[38] Q. Guo, X. Yang, W. Shen, H. Liu, Agglomerate size in an acoustic fluidized bed with sound assistance, Chemical Engineering and Processing: Process Intensification 46 (4) (2007) 307 – 313.

[39] M. Horio, Y. Iwadate, The prediction of sizes of agglomerates formed in fluidized beds, Proceedings of the 5th World Congress of Chemical Engineering, 2nd Intl. Particle Technology Forum V (1996) 571.

[40] M. Leva, Fluidization, McGraw-Hill, New York, 1959.

[41] K. V. Sastry, Similarity size distribution of agglomerates during their growth by coalescence in granulation or green pelletization, International Journal of Mineral Processing 2 (2) (1975) 187 – 203.

[42] H. Hatzantonis, A. Goulas, C. Kiparissides, A comprehensive model for the prediction of particle-size distribution in catalyzed olefin polymerization fluidized-bed reactors, Chemical Engineering Science 53 (18) (1998) 3251 – 3267.

[43] D. Khang, H. H. Lee, Particle size distribution in fluidized beds for catalytic polymerization, Chemical Engineering Science 52 (3) (1997) 421 – 431.

[44] S. K. Friedlander, Smoke, Dust, and Haze: Fundamentals of Aerosol Dynamics, Oxford University Press, 2000.

[45] S. Vemury, S. E. Pratsinis, Self-preserving size distributions of agglomerates, Journal of Aerosol Science 26 (2) (1995) 175 – 185.

[46] E. Limpert, W. A. Stahel, M. Abbt, Log-normal distributions across the sciences: Keys and clues, BioScience 51 (2001) 341–352.

[47] L. Liu, Kinetic theory of aggregation in granular flow, AIChE J 57 (2011) 3331–3343.

[48] L. Liu, Effects of aggregation on the kinetic properties of particles in fluidised bed granulation, Powder Technology 271 (2015) 278 – 291.

Modeling the size distribution in a fluidized bed of nanopowder

Andrea Fabre[a], Samir Salameh[a], Michiel T. Kreutzer[a], J. Ruud van Ommen[a,*]

[a]*Delft University of Technology, Department of Chemical Engineering, Van der Maasweg 9, 2629 HZ Delft, the Netherlands*

Table 1: Properties of the fluidized nanopowders as provided by the manufacturer.

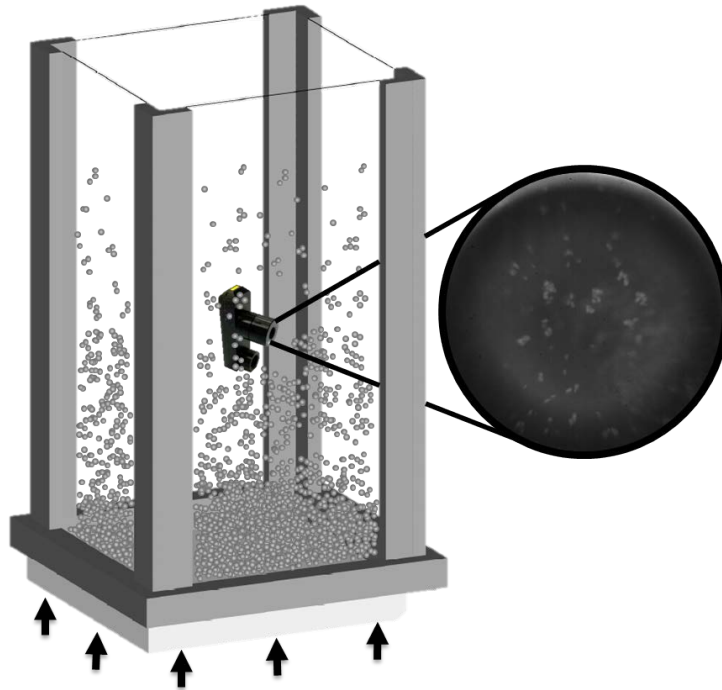| Powder	Surface	d_p (nm)	ρ_p (kg/m^3)	ρ_{Tamped} (kg/m^3)
TiO$_2$ P25	hydrophilic	21	4000	100-180
Al$_2$O$_3$ AluC	hydrophilic	13	3800	50
SiO$_2$ A130	hydrophilic	16	2200	50

Figure 1: *In-situ* analysis of fluidized agglomerates. Nanopowder is fluidized in a square column with the settling tube placed at the splash zone. A sample frame from a recoded video is shown.

*Corresponding author, Tel.: +31 15 27 84393
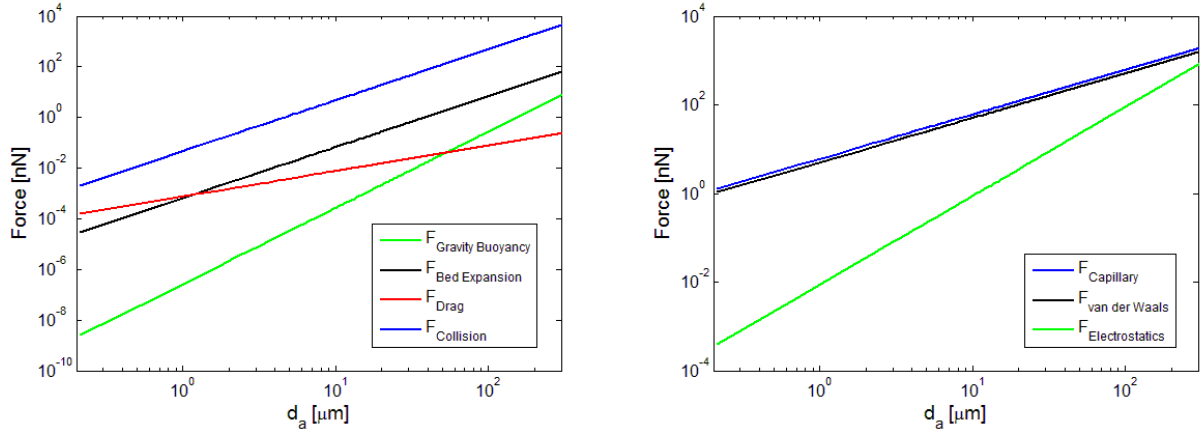   *Email address:* J.R.vanOmmen@tudelft.nl (J. Ruud van Ommen)

Figure 2: Contribution from each force to the overall force balance of agglomerates in a fluidized bed. Left plot corresponds to separation forces; right plot are the adhesion forces. Values were estimated for P25 fluidized with the conditions used in our experiments.

$F_{\text{van der Waals}}$ van der Waals including deformation of soft bodies
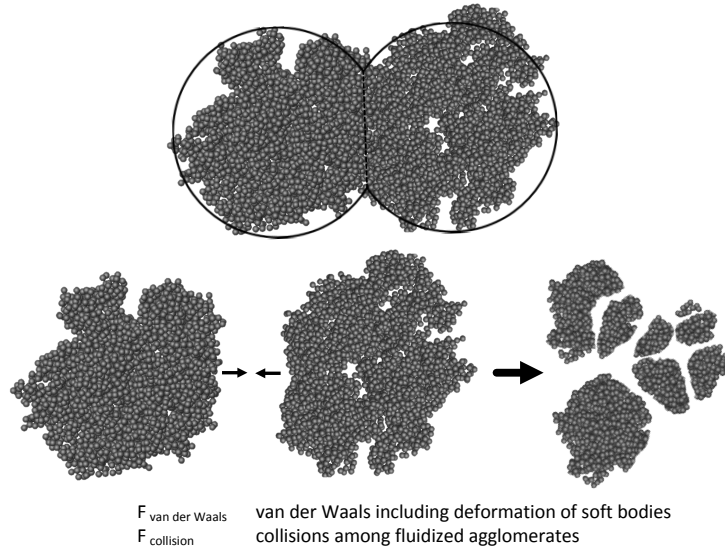$F_{\text{collision}}$ collisions among fluidized agglomerates

Figure 3: Schematic of the force balance on fluidized agglomerates. Van der Waals is the main force holding the agglomerates together, counteracted by the dominant separation force arising from collisions.

Table 2: Number-based average experimental density and size of fluidized agglomerates obtained using the settling tube. Confidence intervals are one standard deviation.

Powder	$\rho_a\ (kg/m^3)$	$d_a\ (\mu m)$
TiO$_2$ P25	101 ± 46	142 ± 66
Al$_2$O$_3$ AluC	55 ± 40	289 ± 173
SiO$_2$ A130	47 ± 26	265 ± 129

Table 3: Properties of the fluidized nanopowders used to estimate coefficients a and b.

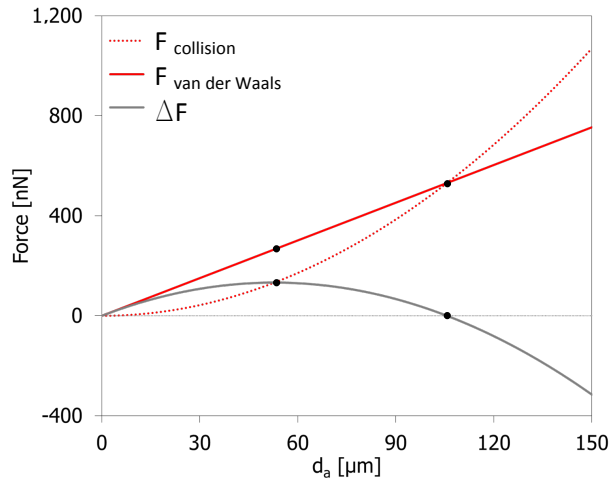| Powder	H_a (J) $\times 10^{-19}$	Young's modulus (GPa)	Work of adhesion (J/m^2)
TiO$_2$ P25	1.02	234	0.8
Al$_2$O$_3$ AluC	1.005	400	5.2
SiO$_2$ A130	0.363	70	0.18

2

Figure 4: Estimation of values used to describe the size distribution inside a fluidized bed of nanopowder. The separation and adhesion forces, together with the force difference versus agglomerate size, are plotted. The circles show the two key values at maximum and zero force difference used by the model to predict the size distribution.

Table 4: Experimental parameters, including representative literature data: μ and σ are the mean and the standard deviation of the log of the distribution, respectively, and δ is the ratio of the mode and the inflection point for the log-normal probability density function. Values for titania (P25), alumina (AluC), and silica (A130, R974) are shown.

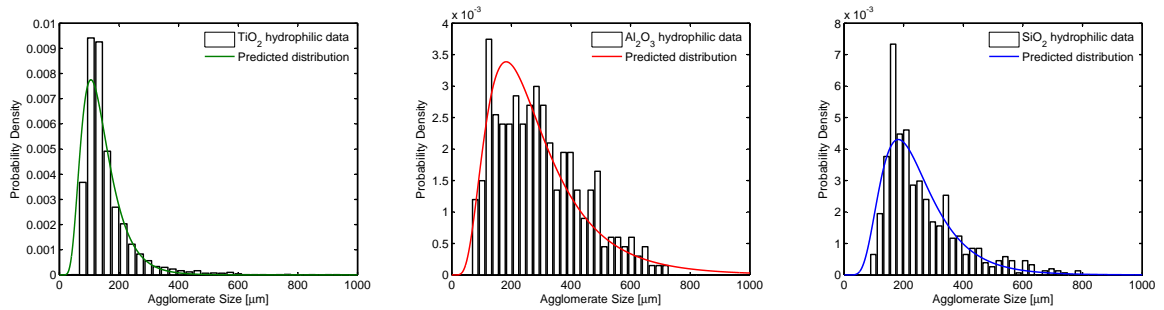| Powder	μ	σ	δ	Fluidization
TiO$_2$ P25	4.86	0.4414	0.58	ABF
Al$_2$O$_3$ AluC	5.51	0.5531	0.48	ABF
SiO$_2$ A130	5.41	0.4584	0.56	APF
TiO$_2$ P25 [10]	4.59	0.5574	0.48	ABF
SiO$_2$ R974 [10]	4.95	0.3698	0.64	APF
SiO$_2$ R974 [22]	4.66	0.4858	0.54	APF

Figure 5: Log-normal prediction of the size distribution for titania (P25), alumina (AluC), and silica (A130). Histogram of raw data and model prediction for each material are plotted.

3